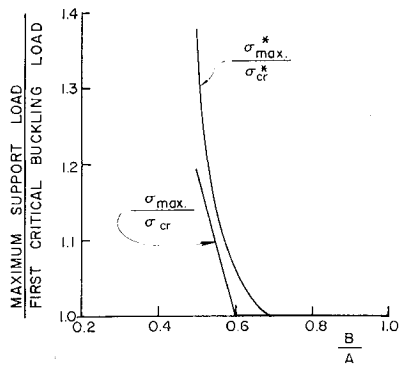

Fig. 11 Effect of eccentricity on maximum load for perfect and imperfect elliptical shells.

shell wall, it was found that the cylinders were sufficiently perfect to buckle close to the predicted classical value based on the circular cylinder equation. In addition, it was observed that significant reductions below the perfect shell buckling loads occurred for the imperfect elliptical cylinders containing small amplitude axial imperfection distributions. Using Koiter's theory for an equivalent axisymmetric imperfect circular cylinder having a radius of curvature R_B, it was shown that the imperfect elliptical cylinder buckling loads could be accurately determined. For large values of eccentricity, maximum compressive loads in excess of the initial buckling load were also noted. In general, it is concluded that elliptical cylindrical shells are indeed sensitive to small geometrical imperfections in shape as predicted by Hutchinson.

References

[1] Kempner, J., "Some Results on Buckling and Postbuckling of Cylindrical Shells," *Collected Papers on Instability of Shell Structures*, TN D-1510, Dec. 1962, NASA.

[2] Kempner, J. and Chen, Y. N., "Buckling and Postbuckling of an Axially Compressed Oval Cylindrical Shell," *Proceedings, Symposium on the Theory of Shells to Honour Lloyd Hamilton Donnell*, Univ. of Houston, McCutchan Publishing Corp., May 1967, pp. 141–183; also PIBAL Rept. 917, April 1966, Polytechnic Institute of Brooklyn.

[3] Hutchinson, J. W., "Buckling and Initial Postbuckling Behaviour of Oval Cylindrical Shells Under Axial Compression," *Transactions of the American Society of Mechanical Engineers, Journal of Applied Mechanics*, March 1968, pp. 66–72.

[4] Kempner, J. and Chen, Y. N., "Postbuckling of an Axially Compressed Oval Cylindrical Shell," *Applied Mechanics Proceedings*, 12th International Congress of Applied Mechanics, Aug. 1968, Stanford Univ.; also Springer-Verlag, New York, 1969, pp. 246–276; also PIBAL Rept. 68-31, Nov. 1968.

[5] Tennyson, R. C. and Muggeridge, D. B., "Buckling of Axisymmetric Imperfect Circular Cylindrical Shells Under Axial Compression," *AIAA Journal*, Vol. 7, No. 11, Nov. 1969, pp. 2127–2131.

[6] Koiter, W. T., "The Effect of Axisymmetric Imperfections on the Buckling of Cylindrical Shells Under Axial Compression," *Proceedings of the Royal Netherlands Academic Sciences*, Amsterdam, Series B, Vol. 66, No. 5, 1963.

[7] Tennyson, R. C., "An Experimental Investigation of the Buckling of Circular Cylindrical Shells in Axial Compression Using the Photoelastic Technique," Rept. 102, Nov. 1964, Univ. of Toronto Institute for Aerospace Studies, Toronto, Ontario, Canada.

[8] Tennyson, R. C., "Photoelastic Circular Cylinders in Axial Compression," *American Society for Testing and Materials*, STP No. 419, 1967, pp. 31–45.

FEBRUARY 1971 AIAA JOURNAL VOL. 9, NO. 2

Turbulent Boundary Layer on a Rotating Disk Calculated with an Effective Viscosity

PAUL COOPER
Case Western Reserve University, Cleveland, Ohio

The incompressible laminar and turbulent boundary-layer flow associated with a rotating disk in an infinite fluid otherwise at rest is calculated. The continuity and two boundary-layer momentum equations are solved by a method adapted from the two-dimensional finite-difference approach of Cebeci and Smith. For the outer portion of the disk where the boundary layer is turbulent, the two Reynolds stress terms involved are replaced by a two-layer scalar eddy viscosity model. Full calculation of boundary-layer development is achieved from the axis of the disk out to a radius corresponding to a rotational Reynolds number $\omega r^2/\nu$ of 10^7. The skewed velocity profiles obtained agree well with experimental data, as do also the results for boundary-layer thickness and skin-friction drag. A kind of three-dimensional turbulent boundary-layer equilibrium appears in a defect similarity of the circumferential mean turbulent velocity profiles.

Nomenclature

A_1, A_2, A_3 = geometrical coefficients in finite-difference expressions
C_M = integrated disk friction moment coefficient = $2M/(\rho\omega^2 R^5/2)$
$c_{f,\theta}$ = circumferential local skin-friction coefficient = $\tau_{w,\theta}/(\rho\omega^2 r^2/2)$
f = radial stream function
g = circumferential stream function
H = shape factor = δ^*/θ
k_1 = von Kármán's constant = 0.4

Received February 18, 1970; revision received August 3, 1970. This research was supported in part by NASA grant NGR 36-003-139. The author wishes to express his appreciation to T. Cebeci and A. M. O. Smith of the McDonnell Douglas Corporation for supplying their computer program and to Dr. Eli Reshotko of Case Western Reserve University and Werner R. Britsch of NASA for their direction and support.

* Graduate Student, Division of Fluid, Thermal and Aerospace Sciences, School of Engineering; also fluids Engineering Specialist at TRW Inc., Cleveland, Ohio.

k_2 = universal constant for the outer layer = 0.0168
M = drag moment of the fluid on one side of disk
n = reciprocal of the power of the mean velocity profile, Eq. (28)
R = radius of outer edge of disk
r = radial coordinate = radius from axis of rotation
R_e = rotational Reynolds number = $\omega r^2/\nu$
$R_{e,\text{o.d.}}$ = outside diameter Reynolds number = $\omega R^2/\nu$
u = mean radial velocity component
$\mathbf{u}$ = mean velocity vector relative to and parallel to disk = $(u, \omega r - v)$
$|\mathbf{u}_e|$ = value of $|\mathbf{u}|$ at edge of boundary = ωr
v = mean absolute circumferential velocity component
w = mean axial velocity component
z = axial coordinate = distance perpendicular to the disk
γ = intermittency factor, Eq. (11)
δ = boundary-layer thickness
δ^* = displacement thickness = $\int_0^\infty (v/\omega r)dz$
η = dimensionless distance perpendicular to disk = $z(\omega/\nu)^{\frac{1}{2}}$
θ = circumferential coordinate = central angle
θ = momentum thickness, Fig. 6
μ = absolute molecular viscosity
ν = kinematic viscosity = μ/ρ
ν_e = effective kinematic viscosity
ρ = fluid density
τ = shear stress
ϕ_f, ϕ_g = improvements to the f and g stream functions, respectively, Eqs. (24) and (26)
ω = angular velocity of disk

Subscripts

i = point on η-grid
k = boundary dividing domains of inner and outer expressions for ν_e, Eqs. (18) and (19)
$n, n-1, n-2$ = stations in the r direction
t = (eddy viscosity) due to turbulence
w = wall = surface of disk
o = fixed value taken from previous iteration
0.995 = value at z where $v = 0.005\omega r$
∞ = far from region of significant variation in u and v
θ = component in circumferential direction

Superscripts

$'$ = differentiation with respect to η; in Eqs. (2) and (3) only, fluctuation component
$+$ = divided by ν

Introduction

NUMERICAL solutions of the turbulent boundary-layer equations have been successfully developed for two dimensions and applied to a variety of flows. Some of these methods use effective viscosity hypotheses to replace the Reynolds stress term. Here the validity of doing this for steady three-dimensional, incompressible boundary-layer flow is investigated. A convenient starting point for such an evaluation is the problem of flow about a smooth, plane disk rotating in an infinite medium otherwise at rest. The characteristically three dimensional, skewed boundary layer is involved, and a considerable amount of test data and theoretical results exists for the problem.

Von Kármán's investigation[1] in 1921 presented a correlation of test data for the drag moment of a rotating disk with his predictions made by a momentum integral method. He used a wall-shear stress relation adapted from the Blasius pipe friction formula and his assumed $\frac{1}{7}$th-power velocity profiles. By assuming logarithmic velocity profiles and the associated law-of-the-wall friction, Goldstein[2] was able to exhibit more closely the trend of the drag moment vs the disk rotational Reynolds number $\omega r^2/\nu$. Theodorsen and Regier[3] obtained test data for the drag moment, which they differentiated to produce the local circumferential skin friction. They also obtained circumferential velocity profiles in the low Reynolds number $\omega r^2/\nu$ range that included transition. Gregory, Stuart and Walker[4] demonstrated that transition from a laminar to a turbulent boundary layer occurs at about $\omega r^2/\nu = 3 \times 10^5$ as one proceeds radially outward on the disk. Cham and Head[5] presented a momentum integral solution that employs circumferential velocity profiles taken from a more recently available two-parameter, turbulent, two-dimensional family and radial velocity profiles from an existing model for the crossflow in three-dimensional boundary layers. By adjustment of the calculated entrainment of fluid into the boundary layer, they were able to produce excellent agreement of the theory with the extensive test data that they obtained on both the disk drag and the associated velocity profiles.

The numerical solution presented here is adapted from the two-dimensional approach of Cebeci and Smith.[6,7] They used separate viscosity assumptions for the inner or wall layer and for the outer layer. A revised version of their implicit, finite-difference method of solving the resulting equations is applied to the present case, which has an additional differential momentum equation. Here we assume that the effective viscosity can be applied as a scalar to the determination of the two turbulent shear-stress components that arise. This was indicated by Mellor[8] who adapted his two-dimensional approach[9,10] to the calculation of the boundary-layer development along the intersection of a stagnation stream surface and a colinear side wall. Therefore, he had to consider the effect of crossflows at this side wall that occurred on both sides of his symmetrical stream surface.

Here we demonstrate that full development of a skewed turbulent boundary layer can be calculated with no assumptions other than the effective viscosity relations and the domain of their application. These are quite general and independent of the flow geometry involved. Results are given for laminar and turbulent flow on the rotating disk for values of the rotational Reynolds number from 0 to 10^7.

Flow Model

The structure of the boundary layers that develop in the neighborhood of a rotating disk is shown in Fig. 1. The disk rotates at constant angular velocity about the z axis of the fixed r-θ-z cylindrical coordinate system in which u, v, and w are the radial, circumferential, and axial components of the mean absolute velocity. The velocity vector relative to the disk has components u, $(\omega r - v)$ and w, and it forms a skewed boundary-layer velocity profile. As with laminar flow, the direction of the wall shear stress relative to the disk is the same as that of $\mathbf{u}$ in the limit as $z \to 0$.

Equations of Motion

The boundary-layer equations for steady incompressible, three-dimensional, axisymmetric, turbulent flow near the rotating disk in the absence of a radial pressure gradient are now given: continuity;

$$(1/r)[\partial(ur)/\partial r] + \partial w/\partial z = 0 \tag{1}$$

momentum in the radial r direction;

$$u(\partial u/\partial r) - (v^2/r) + w\partial u/\partial z = \nu(\partial^2 u/\partial z^2) - (\partial/\partial z)\langle u'w'\rangle \tag{2}$$

and momentum in the circumferential θ direction;

$$u(\partial v/\partial r) + (uv/r) + w\partial v/\partial z = \nu(\partial^2 v/\partial z^2) - (\partial/\partial z)\langle v'w'\rangle \tag{3}$$

The two derivatives of the Reynolds stresses parallel to the

boundary, viz., the last terms of Eqs. (2) and (3), are the only turbulence momentum transport terms remaining after simplifying the Navier-Stokes equations to this boundary-layer form. This leads to Prandtl's assumption that these shear stresses can be related to the mean velocity gradient relative to the wall $\partial \mathbf{u}/\partial z$. Accordingly,

$$\langle u'w' \rangle = -\nu_t \partial u/\partial z \tag{4}$$

and

$$\langle v'w' \rangle = \nu_t[\partial(\omega r - v)/\partial z] = -\nu_t \partial v/\partial z \tag{5}$$

where ν_t is a scalar kinematic eddy viscosity for turbulent flow. Equations (2) and (3) now become

$$u(\partial u/\partial r) - (v^2/r) + w\partial u/\partial z = \partial/\partial z(\nu_e \partial u/\partial z) \tag{6}$$

and

$$u(\partial v/\partial r) + (uv/r) + w\partial v/\partial z = \partial/\partial z(\nu_e \partial v/\partial z) \tag{7}$$

where the scalar effective kinematic viscosity

$$\nu_e = \nu + \nu_t \tag{8}$$

Just as the shear components in three-dimensional laminar flow are simply related to the gradients of the associated velocity components, it is assumed that in three-dimensional, turbulent boundary layers the association of these same gradients with the combined viscous and turbulent shear components maintains the scalar character of the effective viscosity coefficient ν_e.

Effective Viscosity

We now hypothesize that the effective viscosity can be represented by the Smith-Cebeci formulation.[6,7] The inner or wall portion of the boundary layer is characterized by increasing turbulence as one moves away from the wall. Therefore, the effective resistance to shearing of the mean flow (as indicated by ν_e) increases with distance from the wall:

$$\underset{z \leq z_k}{\text{inner layer}\}}\ \nu_e = \nu + k_1^2 z^2 \left|\frac{\partial \mathbf{u}}{\partial z}\right| \left\{1 - \exp\left[-\frac{1}{26}\frac{z}{\nu}(|\tau|/\rho)^{1/2}\right]\right\}^2 \tag{9}$$

where k_1 is the Von Kármán constant (0.4) and $|\tau| = \rho\nu_e |\partial \mathbf{u}/\partial z|$ is the local effective shear stress. The eddy viscosity term ν_t [Eq. (8)] contains an exponential correction that causes ν_e to approach ν as $z \to 0$, which approximates the behavior in the sublayer region. Where the exponential is small (larger z), $\nu_t \to k_1^2 z^2 |\partial \mathbf{u}/\partial z| = l^2 |\partial \mathbf{u}/\partial z|$ where Prandtl's mixing length $l = k_1 z$. Note that $|\partial \mathbf{u}/\partial z| = [(\partial u/\partial z)^2 + (\partial v/\partial z)^2]^{1/2}$. For the outer portion of the layer, Clauser's[11] original suggestion of constant ν_e is modified by an intermittency factor γ:

$$\underset{z \geq z_k}{\text{outer layer}\}}\ \nu_e = \nu + k_2 |\mathbf{u}_e| \delta^* \gamma \tag{10}$$

z_k is the value of z at which the value of ν_e calculated from Eq. (9) becomes equal to that from Eq. (10); $k_2 = 0.0168$; $|\mathbf{u}_e| = \omega r$; and the displacement thickness δ^* is equal to

$$\int_0^\infty (v/\omega r) dz$$

The intermittency is given by

$$\gamma = 1/[1 + 5.5(z/\delta_{0.995})^6] \tag{11}$$

where $\delta_{0.995}$ is the value of z where v differs from zero by 0.005 ωr.

This hypothesis for ν_e is a gross simplifying assumption, because the dynamics of the Reynolds stress tensor are not directly related to gradients of the mean velocity but rather to other turbulence quantities. Nevertheless, in highly sheared flows, it works better than might be expected.

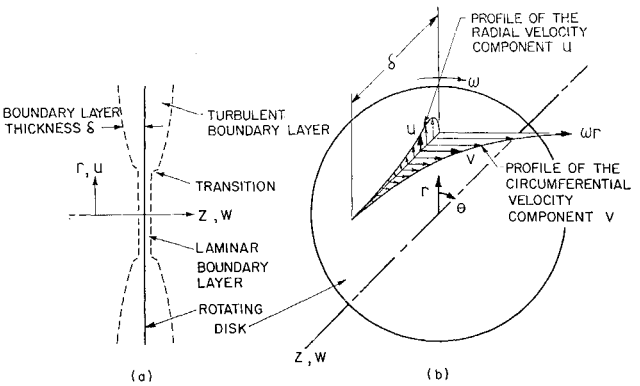

Fig. 1 Coordinate system (r,θ,z) and velocity components (u,v,w); a) indicates the structure and growth of the boundary layer, and b) shows the mean velocity profiles.

Boundary Conditions

The boundary conditions are that at $z = \infty$, $v = u = 0$; and at $z = 0$, $v = \omega r$ and $u = 0$. $\nu_e = \nu$ in the laminar boundary layer that is assumed to exist for $\omega r^2/\nu < R_{e,\text{transition}}$. As is known and will become evident, the dimensionless solution for this laminar layer is independent of radius. The laminar-velocity profiles serve as the starting profiles for the turbulent layer at the chosen radius r corresponding to $\omega r^2/\nu = R_{e,\text{transition}}$. Equations (1, 6, and 7), with the effective viscosity relations of Eqs. (9) and (10), and subject to these boundary conditions constitute the system to be solved for the unknown velocity field (u,v,w). This in turn yields the drag moment $2M$ from the circumferential shear stress $\tau_{w,\theta} = \mu(\partial v/\partial z)_w$, since

$$2M = 2\int_0^R 2\pi r^2 \tau_{w,\theta} dr$$

Transformed Equations and Boundary Conditions

We now eliminate the axial velocity component w by means of the continuity Eq. (1) by introducing stream functions f and g and by transforming the independent variables as follows:

$$z \to \eta,\ r \to r$$

where

$$\eta = z(\omega/\nu)^{1/2} \tag{12}$$

Let

$$g'(\eta, r) = v/\omega r \tag{13}$$

and

$$f'(\eta, r) = u/\omega r \tag{14}$$

where the primes on f and g denote partial differentiation with respect to η. Substitution into the continuity Eq. (1), which is then integrated with respect to η, yields

$$w/(\omega\nu)^{1/2} = -2f - r\partial f/\partial r \tag{15}$$

by setting w and f equal to zero at $\eta = 0$.

The following transformed differential momentum equations are obtained by substituting Eqs. (12) and (15) into Eqs. (6) and (7): r momentum;

$$(\nu_e + f'')' + g'^2 + 2ff'' - f'^2 = r[f'(\partial f'/\partial r) - f''(\partial f/\partial r)] \tag{16}$$

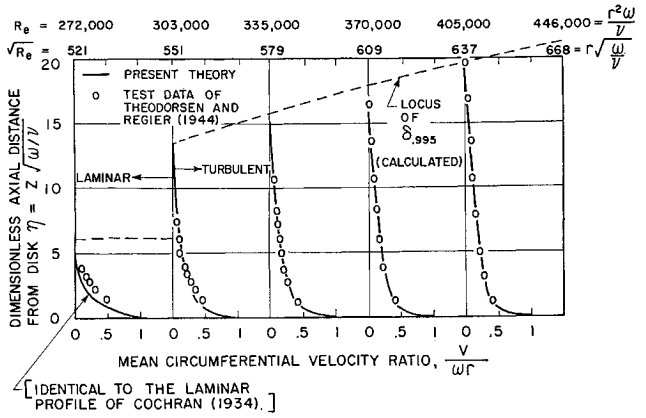

Fig. 2 Development of turbulent mean circumferential velocity profiles; comparison with data from Ref. 3 over a small Reynolds number range that includes transition.

and θ momentum;

$$(\nu_e{}^+ g'')' - 2f'g' + 2fg'' = r[f'(\partial g'/\partial r) - f''(\partial f/\partial r)] \quad (17)$$

where $\nu_e{}^+ = \nu_e/\nu$; and the effective viscosity is given by

$$\text{inner layer}\}\ \nu_e{}^+ = 1 + 0.16\eta^2(R_e)^{1/2}(g''^2 + f''^2)^{1/2} \times \{1 - \exp[-(n/26)(\nu_e{}^+)^{1/2}(R_e)^{1/4}(g''^2 + f''^2)^{1/4}]\}^2 \quad (18)$$

$\eta \leq \eta_k$

(where the value of $\nu_e{}^+$ in the exponential expression is taken from an adjacent point in the η grid of the finite difference scheme to be described);

$$\text{outer layer}\}\ \nu_e{}^+ = 1 + 0.0168(R_e)^{1/2} g_\infty \times 1\Big/\left\{1 + 5.5\left[\frac{\eta}{(\omega/\nu)^{1/2}\delta_{0.995}}\right]^6\right\} \quad (19)$$

$\eta \to \eta_k$

The rotational Reynolds number R_e appears in the $\nu_e{}^+$ expressions in such a way as to require that $\nu_e \to \nu$ as $R_e \to 0$. Note further that in Eqs. (16) and (17) if $\nu_e{}^+$ is independent of r or if $r = 0$, we have another form of the laminar boundary-equations for the rotating disk solved by von Kármán[1] and Cochran.[12] An r independent solution for f and g results, and therefore a constant laminar boundary-layer thickness. Thus the right-hand members of Eqs. (16) and (17) represent the departure from Kármán similarity (viz., the proportionality of the velocity components to ωr at any value of z) that occurs when the boundary layer is turbulent.

The system to be solved for f and g now consists of the two partial differential momentum Eqs. (16) and (17) with $\nu_e{}^+ = 1$ for laminar flow or the appropriate effective viscosity expressions of Eqs. (18) and (19) for turbulent flow. The transformed boundary conditions are that at $\eta = 0$, $f = f' = g = 0$ and $g' = 1$, and that $f' = g' = 0$ at $\eta = \infty$. Also the r-independent laminar solution provides the starting velocity profiles for the turbulent solution (see Fig. 1a). Since the equations are parabolic, and since it is reasonable to assume that the disappearance of the boundary layer beyond the outer edge of the disk (where $r = R$) does not change this character of the equations, no other boundary conditions are needed.

Method of Solution

Next we solve these equations in finite-difference form, being guided by the method of Cebeci and Smith.[6,7] The solution is accomplished implicitly, the calculations advancing radially outward on a grid having arbitrary spacing in the r direction and geometrically increasing spacing in the η direction.

First the momentum Eqs. (16) and (17) are linearized and the r derivatives are replaced by three-point finite-difference formulas at $r = r_n$:

$$(\nu_e{}^+{}_0 f'')' + g_0'^2 + 2f_0 f''' - f_0' f' - r[f_0'(A_1 f' + A_2 f_{n-1}' + A_3 f_{n-2}') - f_0''(A_1 f + A_2 f_{n-1} + A_3 f_{n-2})] = 0 \quad (20)$$

and

$$(\nu_e{}^+{}_0 g'')' - 2f_0' g' + 2f_0 g'' - r[f_0'(A_1 g' + A_2 g_{n-1}' + A_3 g_{n-2}') - g''(A_1 f_0 \times A_2 f_{n-1} + A_3 f_{n-3})] = 0 \quad (21)$$

where the subscript n is implied on all f's, g's and their derivatives except those modified by $n - 1$ and $n - 2$, which denote r stations upstream of r_n. Factors that would otherwise make these equations nonlinear are taken from the previous iteration at the same $r(=r_n)$-station and are so identified by the subscript o.

The A's are given as follows:

$$A_1 = 1/(r_n - r_{n-1}) + 1/(r_n - r_{n-2}) \quad (22a)$$

$$A_2 = -[(r_n - r_{n-2})/(r_n - r_{n-1})(r_{n-1} - r_{n-2})] \quad (22b)$$

$$A_3 = [(r_n - r_{n-1})/(r_n - r_{n-2})(r_{n-1} - r_{n-2})] \quad (22c)$$

Equations (20) and (21) are seen to be linear, ordinary, differential equations in η, because the A's and the quantities having $n - 1$ and $n - 2$ subscripts are known from the solutions at the two previous stations. At small r (as determined by the transition criterion $R_{e,\,\text{transition}} = \omega r_{\text{transition}}{}^2/\nu$) the boundary layer is laminar, and the bracketed terms drop out.

Iterative Procedure

The solution at $r = r_n$ is formed by successively improving an initial estimate of the velocity profiles $f'(\eta, r_n)$ and $g'(\eta, r_n)$. For the first (laminar) station, we assume that $f'(\eta) = 0$ and $g'(\eta)$ varies linearly from 1 at $\eta = 0$ to zero at the chosen value of η_∞. At succeeding stations, we simply start with the results of the previous $(n - 1)$ station.

Representing Eq. (20) by

$$\Gamma(f, f', f'', f'''; \eta, r) = 0 \quad (23)$$

we introduce ϕ_f, the improvement to f_0, as follows:

$$\Gamma = 0 = \Gamma_0 + \phi_f'''\left(\frac{\partial \Gamma}{\partial f'''}\right)_0 + \phi_f''\left(\frac{\partial \Gamma}{\partial f''}\right)_0 + \phi_f'\left(\frac{\partial \Gamma}{\partial f'}\right)_0 + \phi_f\left(\frac{\partial \Gamma}{\partial f}\right)_0 \quad (24)$$

where $\phi_f = f - f_0$, $\phi_f' = f' - f_0'$, etc., and the coefficients of ϕ_f and its derivatives are found from Eq. (20).

Similarly, Eq. (21) is

$$\Lambda(g, g', g'', g'''; \eta, r) = 0 \quad (25)$$

and

$$\Lambda = 0 = \Lambda_0 + \phi_g'''\left(\frac{\partial \Lambda}{\partial g'''}\right)_0 + \phi_g''\left(\frac{\partial \Lambda}{\partial g''}\right)_0 + \phi_g'\left(\frac{\partial \Lambda}{\partial g'}\right)_0 + \phi_g\left(\frac{\partial \Lambda}{\partial g}\right)_0 \quad (26)$$

where the improvement ϕ_g and its derivatives are given by $\phi_g = g - g_0$, $\phi_g' = g' - g_0'$, etc. Equations (24) and (26) are to be solved for the improvements ϕ_f, ϕ_g and their derivatives. It will now be seen that the linearization resulting in Eqs. (20) and (21) was arranged so that only the improvements to f and its derivatives could arise in Eq. (24) and only those to g and its derivatives in Eq. (26). Allowing both ϕ_f's and ϕ_g's to appear in both equations would greatly complicate the numerical procedure.

From this point we follow precisely the Cebeci-Smith procedure[6,7] for finding the ϕ_f's from the differential Eq. (24), and we repeat that procedure a second time to find the ϕ_g's from Eq. (26). Then we accept one-half of these improvements and so modify f_0, g_0 and their derivatives. This constitutes one iteration. The iterations continue until convergence is attained on the quantities δ^* and $(f_w''^2 + g_w''^2)^{1/2}$, the latter being the dimensionless wall shear stress. Then we have a solution at that r station. Briefly, the Cebeci-Smith numerical procedure consists of representing ϕ_f and its derivatives by five-point Lagrange differentiation formulas for a variable grid, where the spacing $\Delta\eta_i = 1.01\,\Delta\eta_{i-1}$ and $\Delta\eta_w = 0.008$, which is the smallest grid spacing in the η direction. Thus, Eq. (24) and the boundary conditions on f and f' become a system of N equations, the unknowns being the set of ϕ_f's at the $N\eta$-points from the wall to the edge of the boundary layer. In matrix form this system is

$$A\phi_f = C \tag{27}$$

The Choleski matrix method[13] is used to solve Eq. (27). The ϕ_g's are found by the same procedure. Five-point means in the η direction are used for the effective viscosities, which are calculated from Eqs. (18) and (19) for turbulent flow.

Calculated Results

By means of the foregoing procedure, we calculated the full development of the boundary layer on a rotating disk with the aid of a digital computer, carrying the calculations from zero radius to that corresponding to $R_e = 1 \times 10^7$. Guided by the experiments of Theodorsen and Regier,[3] we used $R_{e,\,\text{transition}} = 3.04 \times 10^5$, placing two laminar stations ($\nu_e^+ = 1$) at radii less than $r_{\text{transition}}$, and 33 turbulent ones (ν_e^+ given by Eqs. 18 and 19) from there outward. We varied the number of η points from 263 at zero radius to 488 at the last station, making certain that the points of maximum η were well beyond the edge of the boundary layer. About ten iterations were required for a solution at each radial station, the computing time being about one sec per iteration. To facilitate computations and presentation, we used a dimensionless radius $r(\omega/\nu)^{1/2} = (R_e)^{1/2}$, since the Reynolds number is the only controlling parameter in this investigation.

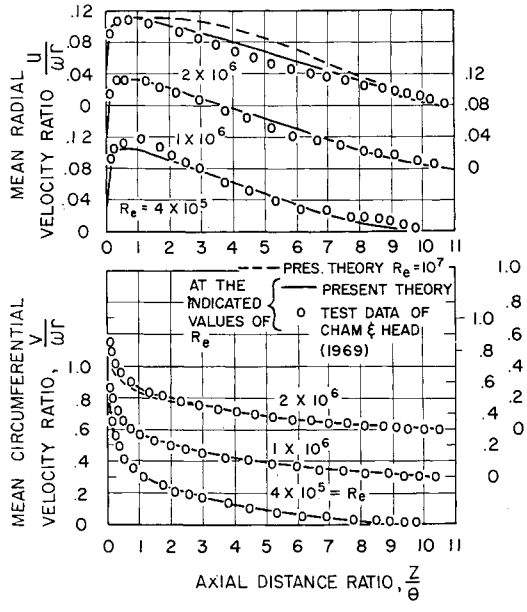

Fig. 3 Turbulent mean radial and circumferential velocity profiles compared with data of Ref. 5; theoretical results at $R_e = 1 \times 10^7$ indicate the development at R_e greater than that of the test data.

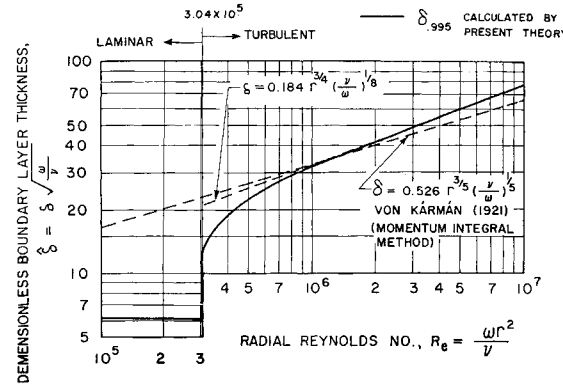

Fig. 4 Boundary-layer thickness $\delta_{0.995}$, which is defined as the value of z at which $v = 0.005\ \omega r$; this calculated growth approaches the proportionality $\delta \alpha r^{3/4}$.

Velocity Profiles

The calculated laminar velocity profiles were identical to those obtained by Cochran.[12] As expected, $u/\omega r$ and $v/\omega r$ [$f'(\eta)$ and $g'(\eta)$, respectively] were independent of r, so that once the solution was found at $R_e = 0$, it was reproduced identically with no further iteration at $R_e = 2.5 \times 10^5$. The circumferential velocity profile thus obtained is shown in Fig. 2. It is compared to test data obtained at $R_e = 272{,}000$ by Theodorsen and Regier[3] who also got these same results at much lower R_e.

The calculated turbulent mean circumferential velocity profiles are compared with test results in both Figs. 2 and 3, where the agreement is good except at the transition (first turbulent) station in Fig. 2. Here the persistence of the laminar trend indicates that transition is not quite so sudden as our method of introducing ν_e from Eqs. (18) and (19) at that point would make it. A more gradual such introduction, as was done by Martellucci et al.,[14] might better reproduce these test results as well as those of the mean radial velocity profile in Fig. 3 at $R_e = 4 \times 10^5$.

On the other hand, these discrepancies could be caused by a breakdown in the validity of the ν_e assumptions near the transition point. The theory used by Cham and Head[5] produced nearly perfect agreement of all velocity profiles with those of their experiments. But to carry out their computations, they first had to make an ad hoc reduction of their entrainment rate from that applicable to two-dimensional boundary-layer calculations. This produced no inconsistencies in their results and could well be applicable to general three-dimensional boundary-layer flow without further adjustment. Nevertheless, the unified effective viscosity approach presented here requires no such adjustments to produce reasonable results for both two-dimensional and—as indicated by the present calculations—three-dimensional boundary layers.

Boundary-Layer Thickness

On Fig. 2, the calculated disk boundary-layer thickness development is indicated for the first few turbulent stations. Figure 4 shows these results for our entire range of Reynolds number. The variation of δ with r approaches an $r^{3/4}$ proportionality at higher R_e, whereas von Kármán's momentum integral results show a proportionality of $r^{3/5}$. (The constant 0.526 is a correction by Goldstein[2] from the original value of 0.462.) This difference arises from von Kármán's restriction to $1/n$th-power mean relative velocity profiles;

$$(\omega r - v)/\omega r = (z/\delta)^{1/n} \tag{28}$$

in which he chose $n = 7$. This requires that his $\delta = (n+1)\delta^*$ where

$$\delta^* = \int_0^\delta (v/\omega r)\,dz$$

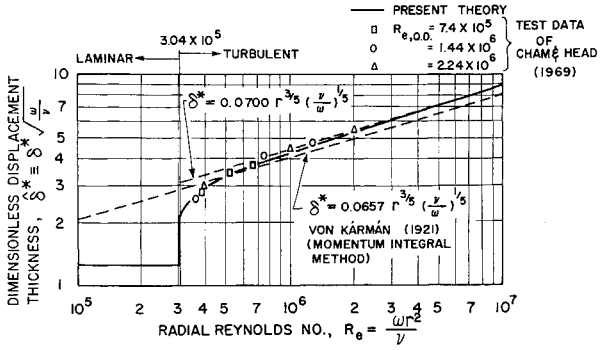

Fig. 5 Displacement thickness δ^* of the circumferential mean velocity profiles, where $\delta^* = \int_0^\infty (v/\omega r)\, dz$; both calculated results and test data asymptotically reveal the same proportionality ($\delta^* \alpha r^{3/5}$) that von Kármán obtained.

Figure 5 compares the results for the displacement thickness. Here the asymptotic behavior of our results and the test data of Ref. 5 give $\delta^* \alpha r^{3/5}$, which is the same as von Kármán obtained. Zero-pressure-gradient, two-dimensional, turbulent, mean velocity profiles possess values of n that increase from 3 to 10 over increasing values of the Reynolds number.[11] Pipe flow has similar behavior. Comparison of our results for δ and δ^* in Figs. 4 and 5 show the same trend.

Figure 6 compares the values of the shape factor H from our theory with the test data of Ref. 5. Our assumption that differing flow conditions at the outer edge of the disk do not affect the results seems justified by these data of Cham and Head in Figs. 5 and 6. Data covering the radial extent of the disk for three different values of the outside diameter Reynolds number $R_{e,\text{o.d.}}$ all fall about on the same line. Thus the radial location of the outer edge of the disk has no noticeable effect on the results at inner radii.

Skin-Friction Drag

The comparison of the local circumferential wall shear stress component results is given in Fig. 7. The data of Theodorsen and Regier[3] at $R = 3 \times 10^5$ indicate that there is some smoothing to the step change exhibited by our calculations that assume sudden transition as discussed previously.

The total skin-friction drag moment M exerted by the fluid on each side of disk is given by

$$M = \int_0^R \tau_{w,\theta}\, 2\pi r^2 dr = \int_0^R c_{f,\theta} \rho \omega r^4 dr \qquad (29)$$

which is plotted dimensionlessly as the moment coefficient C_M in Fig. 8. The results for C_M at $R_{e,\text{o.d.}} > 3 \times 10^5$ are in-

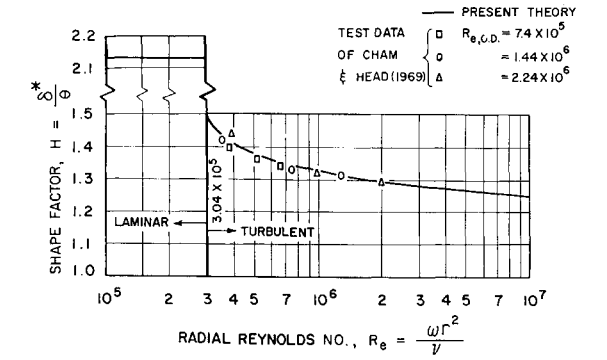

Fig. 6 Shape factor of the circumferential mean velocity profiles. Comparison of calculated results with test data, $H = \delta^*/\theta$, where $\delta^* = \int_0^\infty (v/\omega r)\, dz$ and $\theta = \int_0^\infty (v/\omega r)(1 - v/\omega r)\, dz$.

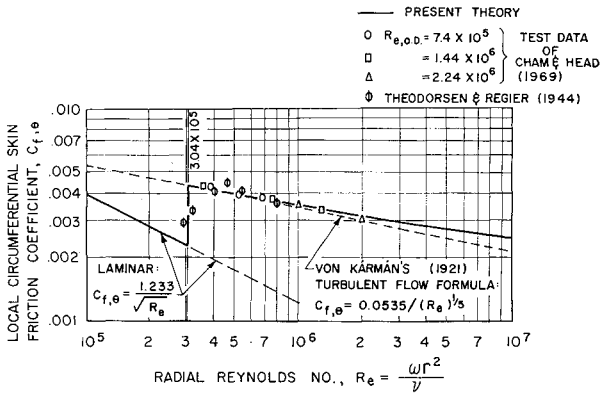

Fig. 7 Circumferential skin-friction component; comparison of theory and experiment; $c_{f,\theta} = \tau_{w,\theta}/(\rho\omega^2 r^2/2)$.

fluenced by the fact that laminar flow exists on those inner portions of these disks for which $R_e < 3 \times 10^5$. This influence is negligible for $R_{e,\text{o.d.}} > 10^6$. The trend at high R_e away from von Kármán's line is at least qualitatively correct. Goldstein[2] derived an expression for C_M, wherein it becomes less dependent on Reynolds number as the latter increases. The same phenomenon is exhibited in pipe friction data and in the drag of two-dimensional equilibrium boundary layers on flat plates.

Similarity

Goldstein's assumption of universal defect profiles $v/(\tau_w/\rho)^{1/2}$ vs z/δ is in agreement with the fact that the same universality emerges in our calculations of $v/(\tau_{w,\theta}/\rho)^{1/2}$ vs z/δ in Fig. 9. Here $v = \omega r - (\omega r - v)$ is the mean circumferential relative velocity defect. Our use of $\tau_{w,\theta}$ rather than τ_w has negligible influence on the outcome, since the angle between τ_w and $\tau_{w,\theta}$ changes only from 17.1° to 10.8° as R_e increases from 4×10^5 to 1×10^7.

We were able to discover no such similarity for the radial mean velocity component nor for its defect $(u_{\text{ref}} - u)$, where u_{ref} is any appropriate reference velocity, which is, say, proportional to ωr. This lack of crossflow similarity may be a characteristic of skewed, turbulent boundary layers.

For two-dimensional turbulent flow, Clauser[11] defined an equilibrium boundary layer as one for which similarity in the defect of the mean velocity (relative to the boundary) exists. We have found similarity of the "free-stream" component of the mean relative velocity defect, which may be the only evidence that one can have of equilibrium in three-dimensional turbulent boundary layers.

Conclusions

A particular example of steady, incompressible, skewed, turbulent, boundary-layer flow has been calculated with

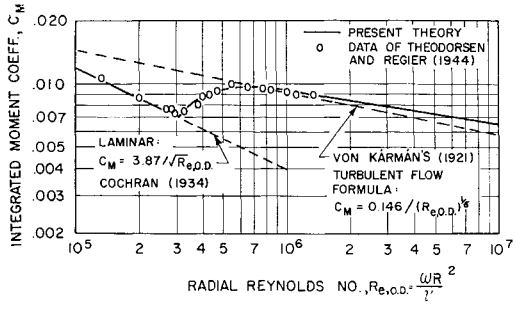

Fig. 8 Integrated moment coefficient due to skin-friction drag; comparison of calculated and experimental results; $C_M = 2M/(\rho\omega^2 R^5/2)$.

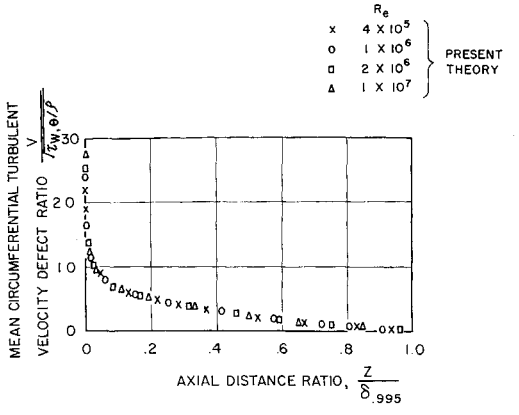

Fig. 9 Defect law investigation; coincidence of circumferential mean velocity profiles when plotted in these defect-law coordinates reveals a state of equilibrium.

reasonable success, using no assumptions other than a hypothesis for a scalar effective viscosity. By applying the molecular viscosity for laminar flow at radii r less than that corresponding to our specified transition value of the Reynolds number $R_e = \omega r^2/\nu = 3.04 \times 10^5$ and Cebeci and Smith's Boussinesq viscosity formulation at greater radii, we have described the flow near a rotating disk in an infinite medium otherwise at rest. Appropriate linearization in the numerical procedure allowed a successful adaptation of their two-dimensional, implicit, finite-difference method to this problem, which involved a second momentum equation.

Using this method we have calculated both laminar and turbulent velocity profiles, displacement thickness, shape factor and drag due to skin friction, obtaining good agreement with theoretical and experimental data. The range of computation extended to $R_e = 1 \times 10^7$.

The results for the drag moment on the disk show the same trends as do those of turbulent drag on flat plates; in fact, the equilibrium behavior of the flat plate boundary layer also appears in a three-dimensional fashion for the rotating disk layer.

Because this is an axisymmetric problem, the form of the equations and the details of the numerical procedure are not much more involved than they are for two-dimensional flow. But the degree of success experienced here indicates that this scalar effective viscosity approach should be applicable to general three-dimensional turbulent boundary-layer flow.

References

[1] von Kármán, Th., "Über laminare und turbulent Reibung," *Zeitschrift für angewandte Mathematik und Mechanik*, Vol. 1, No. 4, Aug. 1921, pp. 244–250; also translation TM 1092, 1946, NACA.

[2] Goldstein, S., "On the Resistance to the Rotation of a Disc Immersed in a Fluid," *Proceedings of the Cambridge Philosophical Society*, Vol. 31, Pt. 11, April 1935, pp. 232–241.

[3] Theodorsen, T. and Regier, A., "Experiments on Drag of Revolving Disks, Cylinders and Streamline Rods at High Speeds," Rept. 793, 1944, NACA.

[4] Gregory, N., Stuart, J. T., and Walker, W. S., "On the Stability of Three-Dimensional Boundary Layers with Application to the Flow due to a Rotating Disk," *Philosophical Transactions of the Royal Society*, Vol. A248, 1955, pp. 155–199.

[5] Cham, T.-S. and Head, M. R., "Turbulent Boundary-Layer Flow on a Rotating Disk," *Journal of Fluid Mechanics*, Vol. 37, Pt. 1, 1969, pp. 129–147.

[6] Smith, A. M. O. and Cebeci, T., "Numerical Solution of the Turbulent-Boundary-Layer Equations," Rept. DAC-33735, May 1967, McDonnell Douglas Corp., Long Beach, Calif.

[7] Cebeci, T. and Smith, A. M. O., "A Finite-Difference Solution of the Incompressible Turbulent Boundary-Layer Equations by an Eddy-Viscosity Concept," Rept. DAC-67130, Oct. 1968, McDonnell Douglas Corp., Long Beach, Calif.

[8] Mellor, G. L., "Incompressible, Turbulent Boundary Layers with Arbitrary Pressure Gradients and Divergent or Convergent Cross Flows," *AIAA Journal*, Vol. 5, No. 9, Sept. 1967, pp. 1570–1579.

[9] Mellor, G. L. and Gibson, D. M., "Equilibrium Turbulent Boundary Layers," *Journal of Fluid Mechanics*, Vol. 24, Pt. 2, 1966, pp. 225–253.

[10] Mellor, G. L., "The Effects of Pressure Gradients on Turbulent Flow near a Smooth Wall," *Journal of Fluid Mechanics*, Vol. 24, Pt. 2, 1966, pp. 255–274.

[11] Clauser, F. H., "The Turbulent Boundary Layer," *Advances in Applied Mechanics*, Vol. IV, Academic Press, New York, 1956, pp. 1–51.

[12] Cochran, W. G., "The Flow due to a Rotating Disk," *Proceedings of the Cambridge Philosophical Society*, Vol. 30, 1934, pp. 365–375.

[13] Hartree, D. R., *Numerical Analysis*, 2nd edition, Oxford University Press, London, 1964, pp. 180–184.

[14] Martellucci, A., Rie, H., and Sontowski, J. F., "Evaluation of Several Eddy Viscosity Models Through Comparison with Measurements in Hypersonic Flows," AIAA Paper 69-688, San Francisco, Calif., 1969.